

CD81 Controls Sustained T Cell Activation Signaling and Defines the Maturation Stages of Cognate Immunological Synapses

V. Rocha-Perugini,^{a,b} M. Zamai,^{b,c} J. M. González-Granado,^b O. Barreiro,^b E. Tejera,^d M. Yañez-Mó,^{a,d} V. R. Caiolfa,^{b,c} F. Sanchez-Madrid^{a,b}

Servicio de Inmunología, Hospital de la Princesa, Instituto de Investigación Sanitaria La Princesa, Madrid, Spain^a; Vascular Biology and Inflammation Department, Centro Nacional de Investigaciones Cardiovasculares, Madrid, Spain^b; San Raffaele Scientific Institute, Milan, Italy^c; Unidad de Investigación, Hospital Santa Cristina, Instituto de Investigación Sanitaria La Princesa, Madrid, Spain^d

In this study, we investigated the dynamics of the molecular interactions of tetraspanin CD81 in T lymphocytes, and we show that CD81 controls the organization of the immune synapse (IS) and T cell activation. Using quantitative microscopy, including fluorescence recovery after photobleaching (FRAP), phasor fluorescence lifetime imaging microscopy-Föster resonance energy transfer (phasorFLIM-FRET), and total internal reflection fluorescence microscopy (TIRFM), we demonstrate that CD81 interacts with ICAM-1 and CD3 during conjugation between T cells and antigen-presenting cells (APCs). CD81 and ICAM-1 exhibit distinct mobilities in central and peripheral areas of early and late T cell-APC contacts. Moreover, CD81-ICAM-1 and CD81-CD3 dynamic interactions increase over the time course of IS formation, as these molecules redistribute throughout the contact area. Therefore, CD81 associations unexpectedly define novel sequential steps of IS maturation. Our results indicate that CD81 controls the temporal progression of the IS and the permanence of CD3 in the membrane contact area, contributing to sustained T cell receptor (TCR)-CD3-mediated signaling. Accordingly, we find that CD81 is required for proper T cell activation, regulating CD3 ζ , ZAP-70, LAT, and extracellular signal-regulated kinase (ERK) phosphorylation; CD69 surface expression; and interleukin-2 (IL-2) secretion. Our data demonstrate the important role of CD81 in the molecular organization and dynamics of the IS architecture that sets the signaling threshold in T cell activation.

The interaction between T lymphocytes and antigen-presenting cells (APCs) is essential for the initiation of the immune response. The dynamic structure formed at cell-to-cell contacts between T cells and APCs, called the immune synapse (IS), is characterized by controlled recruitment of membrane receptors to specific subcellular sites (1). Upon activation by an APC, T cell molecules involved in the IS redistribute in highly organized structures at the T cell-APC contact (2). The T cell receptor (TCR) and associated molecules concatenate into the central area (central supramolecular activation cluster [cSMAC]), whereas adhesion receptors rearrange in a surrounding external ring called the peripheral supramolecular activation cluster (pSMAC) (3). During IS formation, preclustered TCR “protein islands” converge into larger aggregates that translocate toward the cSMAC (4, 5), from where they are internalized and degraded (6). The balance between the generation and degradation of TCR microclusters is critical for sustained T cell activation (5, 7) and is modulated by ligand mobility (8). However, the mechanisms regulating protein receptor movement and the basis for IS molecular segregation are still poorly understood.

A plethora of molecules are translocated to the IS during T cell activation (9). These include the tetraspanins CD81 (10) and CD82 (11), which are known to associate with several IS components such as major histocompatibility complex class II (MHCII) molecules, CD4, and LFA-1 (12–15). However, the specific role of tetraspanins in the IS remains unknown. Tetraspanins are ubiquitous proteins that modulate the function of their associated partners and play important roles in a wide variety of physiological and pathological processes, including immunity and inflammation (16). They interact with each other and with other receptors, cytoskeletal components, and signaling molecules, acting as organizers of molecular macrocomplexes called tetraspanin-en-

riched microdomains (TEMs) (17). The existence of TEMs has been demonstrated by biochemical approaches (16, 18) and by single-molecule fluorescence techniques in living cells (19, 20). In the immune system, it has been shown that CD81 provides a costimulatory signal in T cells, associates with CD19, and facilitates antigen presentation by associating with MHCII molecules in APCs (21). Mice deficient for CD81 have hyperactive B cells (22), delayed humoral immune responses, impaired T helper type 2 responses, and hyperproliferative T cells (21). In T cells, TEM insertion has been demonstrated for CD4 and CD8 coreceptors (13, 23) and for VLA-4 and LFA-1 integrins (15, 24). ICAM-1, the adhesion receptor ligand for the LFA-1 integrin, is also a TEM component, mediating intercellular adhesion (25). Although ICAM-1 has been thoroughly studied on APCs, ICAM-1 and LFA-1 are present on both APCs and T lymphocytes. ICAM-1 expression on T cells (26–28) and LFA-1 expression on APCs (29, 30) can also play a role in T cell-APC contact (31–36). Moreover, CD81 cross-linking stimulates LFA-1-ICAM-1-mediated thymocyte aggregation (37) and promotes T cell-B cell interactions by activating LFA-1 integrin (38). Thus, tetraspanins might have an important role in IS organization.

Received 12 March 2013 Returned for modification 8 April 2013

Accepted 3 July 2013

Published ahead of print 15 July 2013

Address correspondence to F. Sanchez-Madrid, fsanchez.hlpr@salud.madrid.org.

Supplemental material for this article may be found at <http://dx.doi.org/10.1128/MCB.00302-13>.

Copyright © 2013, American Society for Microbiology. All Rights Reserved.

doi:10.1128/MCB.00302-13

Here, we investigated the role of the tetraspanin CD81 as an IS organizer in live T cell-B cell conjugates. Using state-of-the-art microscopy approaches, we show that CD81 is a critical regulator of the IS architecture on the T cell side of the T cell-APC contact. Our data also reveal that CD81 controls the staging of IS maturation through its interaction with CD3 and ICAM-1. This is due, at least in part, to its role in controlling CD3 clustering and permanence at the IS. Thus, CD81 is a critical regulator of CD3 clustering, sustained CD3 signaling, and T cell activation.

MATERIALS AND METHODS

Antibodies, reagents, peptides, and recombinant DNA constructs. Poly-L-lysine (PLL), influenza virus hemagglutinin (HA) peptide, and unconjugated and fluorescein isothiocyanate (FITC)-conjugated anti- α -tubulin were obtained from Sigma. *Staphylococcus enterotoxin E* (SEE) was obtained from Toxin Technology. Alexa Fluor 488 and 647, streptavidin-Alexa Fluor 488, rhodamine X, phalloidin-Alexa Fluor 488 and -Alexa Fluor 647, anti- α -tubulin-Alexa Fluor 647, and the cell tracker CMAC (7-amino-4-chloromethylcoumarin) were obtained from Invitrogen. The antibodies (Abs) T3b (anti-CD3), TP1/40 (anti- α L integrin), TS1/18 (anti- β 2 integrin), HU5/3 (anti-ICAM-1), TP1/55 (anti-CD69), VJ1/20 (anti-CD9), LIA1/1 (anti-CD151), HP2/6 (anti-CD4), and T200 (anti-CD45) were produced in our laboratory. CD81 monoclonal Ab (MAB) 5A6, CD3 ζ polyclonal Ab (pAb) 448, CD82 MAb TS82b, and MEM53 MAb CD53 were kindly provided by S. Levy (Stanford, CA, USA), B. Alarcón (CBM, Spain), E. Rubinstein (Institut André Lwoff, Villejuif, France), and V. Horejsí (Czechoslovak Academy of Sciences, Prague, Czech Republic), respectively. Antibodies against phospho-phospholipase C- γ (phospho-PLC- γ) (Y783), PLC- γ , phospho-ZAP-70 (Y493), and phospho-Erk1/2 (T202/Y204) were obtained from Cell Signaling. ZAP-70 Ab, LAT Ab, phospho-CD3 ζ (Y83), and phospho-LAT (Y132) were obtained from Abcam. Erk1/2 Ab was obtained from Millipore, and CD69-allophycocyanin was obtained from BD Biosciences.

Tetramethylrhodamine (TAMRA) N-terminally labeled peptides with the sequence RRRRRRCCGIRNSSVY (CD81) or RRRRRRRYSVNICR GCSS (scrambled) were purchased from LifeTein (South Plainfield, NJ, USA). Glutathione S-transferase (GST) alone and GST-LEL-CD81 peptides were prepared as described previously (25).

For the CD81-mCherry construct (with the mCherry tag at the C-terminal domain), a CD81 PCR product was subcloned into pEGFP-C1 (Invitrogen), in which the enhanced green fluorescent protein (EGFP) sequence was replaced by the monomeric Cherry (mCherry) sequence. This construct was kindly provided by E. Rubinstein. The constructs pEGFP-N1-CD3 ζ (39), provided by B. Alarcón; CD9-mEGFP; and ICAM-1-mEGFP (19) were previously described. ICAM-3 tagged with monomeric EGFP (mEGFP) was obtained from ICAM-3-EGFP (40) by using a QuikChange Multi site-directed mutagenesis kit from Stratagene (La Jolla, CA, USA).

Cells and cell culture. V β 8 Jurkat T cell clones (J77) and the lymphoblastoid Raji and Hom2 (HLA-DR1 Epstein-Barr virus [EBV]-transformed) cell lines were cultured in RPMI 1640 medium (Sigma) supplemented with 10% fetal calf serum (FCS; Invitrogen), and HEK293T cells were cultured in Dulbecco's modified Eagle's medium (DMEM) (Sigma) supplemented with 10% FCS. HA-specific V β 3 Jurkat T cells (CH7C17) were supplemented with 400 μ g/ml hygromycin B (Invitrogen) and 4 μ g/ml puromycin (Sigma). Stable cell populations overexpressing CD81-mCherry or ICAM-1-mEGFP were generated by transfection and selection with 1 mg/ml G418 (Invitrogen).

Peripheral blood lymphocytes from healthy donors were isolated by Ficoll-Hypaque gradient centrifugation and cultured for 2 days in RPMI 1640 medium supplemented with 10% fetal bovine serum (FBS) (Cambrex Bioscience) and SEE (0.1 μ g/ml). Isolated T lymphoblasts were then maintained in culture for 5 days in the presence of interleukin-2 (IL-2) (50 U/ml).

Cell transfection and silencing. J77 cells (2×10^7) were washed twice with Hanks' balanced salt solution (HBSS) (Lonza) and transiently transfected by electroporation with plasmids (20 μ g) or cotransfected with plasmids (10 μ g) and small interfering RNA (siRNA) (1 μ M) in OptiMEM medium (Gibco, Invitrogen) at 240 V and 32 ms (Gene Pulser II; Bio-Rad). Control siRNA and siRNA for CD81 (siCD81) (CACGTCG CCTTCAACTGTA) were purchased from Eurogentec.

For lentiviral silencing of endogenous CD81, short hairpin RNA (shRNA) lentiviruses were produced by cotransfection of HEK293T cells (Lipofectamine 2000; Invitrogen) with pLVX-shRNA2 (with Zsreen fluorescence; Clontech), encoding the shRNA sequence (the same sequence as siCD81), or with an empty plasmid as a control, together with plasmids pCMV- Δ R8.91 and pMD2.G-VSV-G. Supernatants were collected after 48 to 72 h and filtered (0.45 μ m; Millipore). J77 or CH7C17 cells were spin infected for 2 h at $1,200 \times g$ and incubated for 4 h at 37°C. Two rounds of transduction were performed at 24-h intervals, and experiments were carried out after a further 48 h. Results were confirmed with two independent sequences of shRNA to control for off-target effects. siRNA or shRNA knockdown was tested by flow cytometry at 48 h posttransfection.

Conjugate formation. B cells (Raji or Hom2) were loaded with the CMAC tracker and loaded with SEE (0.5 to 1 μ g/ml) or HA peptide (100 to 200 μ g/ml), as appropriate (41). J77 or CH7C17 T cells were mixed with Raji or Hom2 B cells (1:1), centrifuged at low speed to favor conjugate formation, and incubated at 37°C for the indicated periods of time.

CH7C17 T cells were incubated for 3 h at 37°C with 10 μ M permeable CD81 or scramble peptides or alternatively with 150 μ g/ml of GST alone or the GST-LEL-CD81 fusion protein. Pretreated T cells were then conjugated with Hom2/HA B cells for 16 h at 37°C, stained with antibodies against CD69, and analyzed by flow cytometry.

Flow cytometry. Cells were cocultured in 96-well plates at 37°C for the indicated periods. After staining of cells with specific antibodies, data were acquired with a FACSCantoII flow cytometer (BD) and then analyzed with BD FACSDIVA (BD) or FlowJo software (FlowJo Inc.). B cells were distinguished by CMAC staining, and in shRNA experiments, T cells were distinguished by Zsreen fluorescence.

To measure F-actin content, J77 cells were stimulated for different times with 10 μ g/ml purified anti-CD3 (T3b), fixed in 2% paraformaldehyde (PFA), permeabilized in 0.5% Triton X-100 in phosphate-buffered saline (PBS), and labeled with phalloidin. All experiments were performed in triplicates.

IL-2 production. shRNA-transduced J77 T cells were conjugated with SEE-loaded Raji B cells. For measurement of IL-2 secretion, supernatants were harvested after 16 h, and IL-2 content was measured by using the IL-2 ELI-pair kit (Diaclone).

Immunoblotting. shRNA-transduced J77 T cells were conjugated with SEE-loaded Raji B cells (10:1) for the indicated times and lysed with 1% Triton X-100 in PBS containing Complete protease and PhoSTOP phosphatase inhibitors (Roche). Proteins were separated by SDS-PAGE, and proteins were revealed with the Fujifilm LAS-3000 imaging system after membrane incubation with specific antibodies and peroxidase-conjugated secondary antibodies. Band intensities were quantified by using Metamorph software (Molecular Devices), and results were normalized to the total protein expression level.

Fluorescence confocal microscopy. For immunofluorescence, T cell-B cell conjugates formed by incubation for different times at 37°C were allowed to adhere onto PLL-coated coverslips (40 μ g/ml) for 15 min at 37°C and fixed in 4% PFA (Electron Microscopy Sciences). Samples were fixed, stained with appropriate primary antibodies followed by species-matching secondary antibodies or streptavidin (when primary antibodies were biotinylated) coupled to Alexa Fluor fluorochromes (Invitrogen), and mounted in Prolong antifade medium (Invitrogen). To detect intracellular proteins, cells were first permeabilized with PBS-0.5% Triton X-100 for 5 min.

For live-cell imaging, microscopes were fully covered by an acrylic box to allow analysis at 37°C in 5% CO₂. For time-lapse fluorescence imaging,

cells were resuspended in HBSS (Lonza)–2% FCS—20 mM HEPES (Lonza), plated onto PLL-coated 35-mm dishes (MatTek), and maintained at 37°C in 5% CO₂.

Confocal images were obtained with a Leica TCS-SP5 confocal scanning laser unit attached to an inverted epifluorescence DMI6000B microscope fitted with an HCX PL APO lambda blue 63×/1.4-numerical-aperture (NA) oil immersion objective, using Las-AF acquisition software (Leica Microsystems), or alternatively with a Zeiss LSM700 confocal scanning laser unit attached to an inverted epifluorescence microscope (Observer.Z1) fitted with a Plan APO Chromat 63×/1.4-NA oil immersion objective, using ZEN 2009 acquisition software (Carl Zeiss Microscopy GmbH). Images were analyzed with Leica LAS-AF, Metamorph, or ImageJ software (NIH).

Protein relocation to the IS was quantified with the SynapseMeasure plug-in in ImageJ (42). Briefly, the quantification takes into account the fluorescence intensity signals measured in selected regions with similar areas at the T cell-APC contact zone (IS), the APC membrane not in contact with the T cell (B), the T cell membrane not in contact with the APC (T), and the background (Bg). Bg signal was subtracted from all other measurements, and signal accumulation at the IS relative to the rest of the T cell surface was then analyzed according to the formula $(IS - B)/T$. In the charts, each dot corresponds to a T cell-B cell conjugate.

Measurements of Pearson's coefficient for the colocalization of CD3ζ-mEGFP and CD81-mCherry or ICAM-1-mEGFP and CD81-mCherry were performed with Imaris (Bitplane). We analyzed the three-dimensional (3D) IS contact area from time-lapse stack confocal microscopy videos. For each cell-cell conjugate, measurement of GFP-Cherry colocalization was performed considering for all confocal stacks only the 1 μm closest to the Raji B cell membrane.

Fluorescence recovery after photobleaching (FRAP). J77/CD81-mCherry or J77/ICAM-1-mEGFP cells were incubated with Raji/SEE cells for 2 min and plated for 5 min onto PLL-coated coverslips. Live-cell microscopy was performed at 37°C in 5% CO₂ with a Nikon A1-R multiline confocal scanning unit coupled to an Eclipse Ti microscope fitted with a PL APO 60×/1.4-NA oil immersion objective, the 488-nm Ar laser line for ICAM-1-mEGFP, or the 561-nm diode laser line for CD81-mCherry. Bleaching was conducted on membrane areas of the central or pSMAC of the early and late IS and on comparable areas of the plasma membrane of nonconjugated T cells. Laser power for bleaching was maximal but was reduced to 10% for imaging. At the optimal focal plane, the acquisition protocol was as follows: 10 prebleach images, 1 s of iterative bleach pulse, 60 images at 1-s intervals, 30 images every 10 s, and 3 images every 30 s (256 by 256). Fluorescence recovery in the bleached region (8.4 μm² for ICAM-1-mEGFP and 8.94 μm² for CD81-mCherry) was measured as the average signal intensity. All recovery curves were generated as described previously (19). The averaged recoveries were fitted by using a simple Brownian diffusion model with GraphPad Prism. Statistical analyses were performed on the raw data for each protein and each condition. The immobile fractions and half-recovery times were determined from the fitted curves.

Hetero-Föster resonance energy transfer (FRET) by donor phasor fluorescence lifetime imaging microscopy (phasorFLIM) in intact living cells. J77 T cells were transiently cotransfected with proteins fused to monomeric EGFP (ICAM-1-mEGFP, CD3ζ-mEGFP, CD9-mEGFP, or ICAM-3-mEGFP) and CD81-mCherry by electroporation. After 24 h, cells expressing intermediate levels (mean fluorescence intensity at fluorescence detector FL-2 of 10² to 10⁴) of mEGFP-tagged protein and high levels (mean fluorescence intensity at FL-1 of 10³ to 10⁵) of CD81-mCherry were sorted on a FACSAriaII flow cytometer (BD) and cultured for at least 2 h. Cells were then incubated with Raji/SEE cells for 2 min and plated for 10 min onto PLL-coated 35-mm dishes at 37°C (MatTek) before analysis. CMAC was used at a 100-times-lower concentration than that used for other experiments to avoid interference with EGFP fluorescence under multiphoton excitation.

FLIM images were collected at 37°C in 5% CO₂ in raster scanning

mode using a 2-channel Alba spectrometer (ISS Inc.) combined with a digital frequency domain (DFD) fast-FLIM card (ISS Inc.) and equipped with H7422 fast photomultipliers (Hamamatsu Photonics). The ALBA module was coupled to an inverted Nikon Ti-E microscope (Nikon Corp.) equipped with a Nikon MRD07600 CFI 60×/1.2-NA WI Plan Apochromatic objective, an epifluorescence lamp, a bright field, a top-stage incubator, and a heating chamber (Okolab SRL). Excitation at 830 nm was provided by a femtosecond-pulsed mode-locked tunable MaiTai DeepSee laser (Newport Corp.). Emission signals were collected after blocking with FF01-680/SP and BP530/43 filters (Semrock Inc., IDEX Corporation). The laser power at the objective was 10 mW. A series of 20 to 50 consecutive 256-by-256-pixel images at 64 μs/pixel were averaged. Phasor analysis was carried out by using SimFCS (Globals Unlimited, LFD). We analyzed the dispersion of the donor fluorophore alone in the phasor plot to determine the size of the cursor and considered only the pixels identified outside the distribution of the donor-only cells (43). For each mEGFP-mCherry pair of proteins, the highest FRET efficiency was selected (27% for CD81-CD9, 23% for CD81-ICAM-1, and 22% for CD81-CD3), always maintaining the same cursor size, and the number of pixels inside the cursor was quantified.

TIRFM. J77 T cells were cotransfected with CD3ζ-mEGFP and control or CD81 siRNA, sorted on a FACSAriaII flow cytometer, cultured for 24 h, and plated onto 35-mm dishes (MatTek) coated with 10 μg/ml purified anti-CD3 (T3b). Images were acquired for 10 min at 0.35-s intervals on a Leica AM total internal reflection fluorescence microscopy (TIRFM) multicolor unit mounted on a Leica DMI6000B microscope fitted with a 100×/1.46-NA oil immersion objective, using a ×1.6 magnification and ~90-nm depth penetration (analysis of microclusters at the cell membrane). Images were analyzed with Imaris (Bitplane). For the analysis of CD3 cluster movement, background was subtracted by using the local contrast threshold. The minimum cluster diameter was then estimated to be 0.4 μm, and a Brownian motion algorithm was applied, considering 2 μm as the maximum distance of cluster displacement and no gaps between frames. For the analysis of cSMAC areas, absolute intensity was used for thresholding.

Statistical analysis. All statistical analyses were performed with GraphPad Prism (GraphPad Software Inc.). *P* values were calculated by using two-tailed Student's *t* test or, when specified, one-way analysis of variance (ANOVA) with Bonferroni's or Tukey's (for analysis of variance) *post hoc* multiple-comparison test. Statistical significance was assigned at *P* values of <0.05 (indicated by * in the figures), <0.01 (indicated by **), and <0.001 (indicated by ***).

RESULTS

CD81 dynamics during IS progression. To test the potential role of CD81 in membrane protein reorganization during IS formation, we first assessed CD81 redistribution during T cell-B cell conjugation, comparing it to the redistribution of markers of the cSMAC (CD3ζ) and pSMAC (ICAM-1). Primary human T lymphoblasts were conjugated with Raji B cells labeled with CMAC cell tracker and loaded with superantigen E (Raji/SEE cells) for different times, plated onto poly-L-lysine-coated coverslips for 10 min, fixed, and stained with antibodies against CD81 and CD3 or CD81 and ICAM-1 (Fig. 1). CD81 was enriched at the IS, colocalizing with CD3 at the cSMAC in 10-min conjugates, while ICAM-1 was enriched at the pSMAC. In later conjugates, after 30 min of cell-cell contact, CD81 and ICAM-1 were equally distributed throughout the IS, while CD3 remained accumulated at the cSMAC (Fig. 1).

To further investigate the dynamics of CD81 redistribution at the IS during T cell-B cell conjugation, J77 T cells cotransfected with CD81-mCherry and CD3ζ-mEGFP were conjugated with Raji/SEE cells, and conjugates were analyzed by time-lapse confocal microscopy (Fig. 2). CD81 relocated to the IS within the first

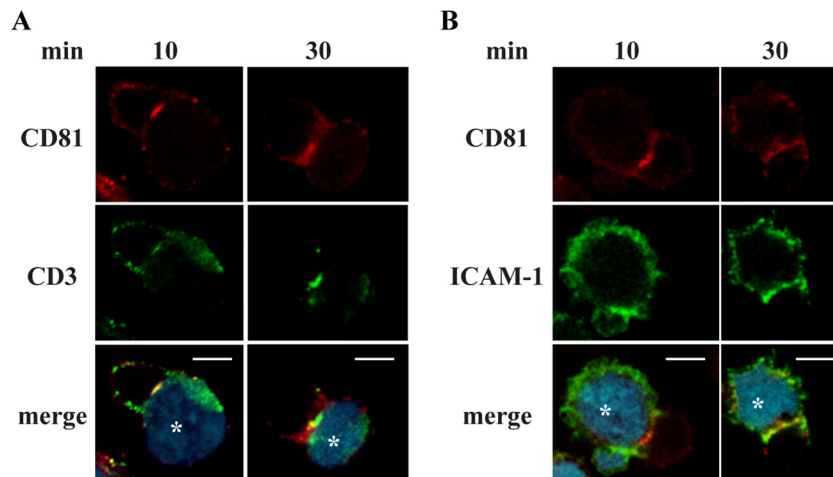


FIG 1 CD81, CD3, and ICAM-1 enrichment at the IS. Primary human T lymphoblasts were conjugated with CMAC-labeled SEE-loaded Raji B cells (blue) (asterisks) for 10 or 30 min. Cells were then plated onto PLL-coated coverslips, fixed, and stained with antibodies against CD81 (red) and CD3 or ICAM-1 (green). A single confocal plane is shown. Bars, 10 μ m.

minutes of conjugation, colocalizing with CD3 at the cSMAC, and remained in this location for up to 20 min (Fig. 2A). Quantification of CD81-mCherry and CD3-mEGFP Pearson's coefficients at the 3D IS contact area showed high levels of colocalization at all times analyzed (Fig. 2A, right). To compare the dynamics of CD81 redistribution at the IS with a pSMAC marker, we used the adhesion molecule ICAM-1, since fluorescently tagged integrins were not stable and did not show proper subcellular distribution (data not shown), precluding its use in studies based on fluorescence microscopy. Although ICAM-1 is typically seen as a pSMAC component at the APC side and is highly expressed on APCs, it is also endogenously expressed by T cells (see Fig. S1A in the supplemental material). In addition, Raji and Hom2 B cells, used as APCs, endogenously expressed the integrin LFA-1 ($\alpha_1\beta_2$) (see Fig. S1B in the supplemental material). J77 T cells were cotransfected with CD81-mCherry and ICAM-1-mEGFP and conjugated with Raji/SEE cells (Fig. 2B). During the initial phase of the early IS, CD81 but not ICAM-1 was enriched at the central area (Fig. 2B). Quantification of ICAM-1-mEGFP and CD81-mCherry Pearson's coefficients at the contact area in time-lapse videos indicated that CD81-ICAM-1 colocalization was enhanced with the time of conjugation, reaching a peak by 10 min of cell-cell contact (Fig. 2B, right). Indeed, by that time, ICAM-1 started to relocate throughout the IS. At later times, after \sim 20 min, CD81 was also redistributed from the cSMAC so that ICAM-1 and CD81 proteins colocalized at the entire cell-cell contact (Fig. 2B). Likewise, CD3 exhibited a similar redistribution pattern after \sim 50 min (Fig. 2C). We could therefore define an early stage in the IS in which CD81 and CD3 colocalized at the cSMAC while ICAM-1 was located at the pSMAC and a late IS in which all three receptors redistributed along the entire IS cell-cell contact. These data suggest that CD81 might be important in the initiation of antigen-triggered CD3 clustering.

We next investigated the mobility of CD81 at the IS by using FRAP (fluorescence recovery after photobleaching). J77/CD81-mCherry T cells were conjugated with Raji/SEE cells, and the cSMAC or pSMAC membrane areas of T cells were bleached during early or late IS formation (Fig. 3A). Fluorescence recovery under each condition was measured, and the immobile fractions

and half-recovery times of the mobile fractions were obtained from the fitted curves. The apparent diffusion coefficients in control nonconjugated T cells and in different areas and phases of the IS were also calculated (Table 1). We found that a greater proportion of CD81 molecules were immobile at the early IS cSMAC than at the cell membrane of control nonconjugated T cells, whereas the immobile fraction at the pSMAC was similar to that in control cells, indicating that CD81 is confined mostly to the early IS cSMAC (Fig. 3B and D). In both areas of the early IS, the diffusion dynamics of mobile CD81 molecules remained similar to those in control cells (Fig. 3B and E and Table 1), as indicated by the half-recovery times and the calculated apparent diffusion coefficients. In the late IS, the CD81 immobile fraction increased in both the cSMAC and pSMAC with respect to nonconjugated cells (Fig. 3C and D). Moreover, the mobile CD81 molecules showed a slower mobility than in control cells (Fig. 3C and E and Table 1), suggesting a general decrease in diffusion consistent with more stable protein-protein interactions in both areas.

We compared the observed CD81 dynamics with that of ICAM-1, which is included in TEMs (25). J77/ICAM-1-mEGFP T cells conjugated with Raji/SEE cells were bleached at the cSMAC or pSMAC during early or late IS formation (Fig. 3F). FRAP analysis revealed a higher ICAM-1 immobile fraction in the early IS pSMAC than in nonconjugated T cell membranes (Fig. 3G and I), and mobile molecules entering this area moved more slowly (Fig. 3G and J and Table 1). ICAM-1 dynamics in the early IS cSMAC was similar to that in control cells (Fig. 3G, I, and J and Table 1), indicating that ICAM-1 is confined mostly to the early pSMAC. In the late IS, both areas showed reduced diffusion dynamics in comparison to those in nonconjugated cells, but more ICAM-1 molecules were immobile in central than in peripheral areas, suggesting stronger interactions (Fig. 3H to J and Table 1).

CD81 molecular interactions within TEMs define IS maturation stages. We then assessed in living cells the dynamics of protein-protein interactions at the contact area during IS maturation by using phasorFLIM-Föster resonance energy transfer (FRET) (43, 44). J77 T cells were cotransfected with monomeric EGFP-tagged proteins (43, 45) as the donor (CD9-mEGFP, ICAM-1-mEGFP, or

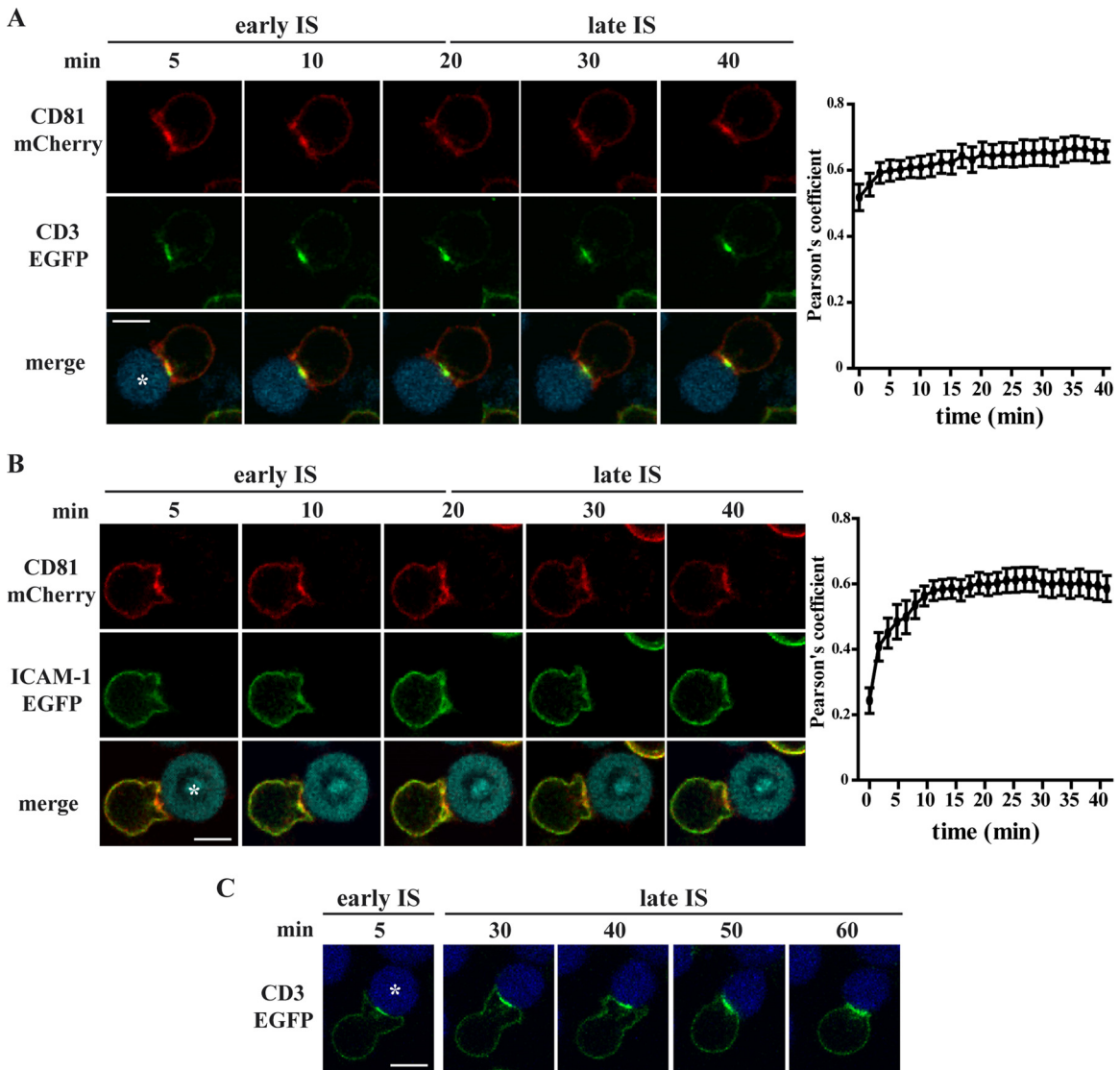


FIG 2 CD81, CD3, and ICAM-1 relocalization depends on IS maturation. J77 cells transfected with CD81-mCherry and CD3 ζ -mEGFP (A), CD81-mCherry and ICAM-1-mEGFP (B), or CD3 ζ -mEGFP (C) were conjugated with Raji/SEE cells (blue) (asterisks). Cells were monitored by time-lapse confocal microscopy at \sim 1.5-min intervals. A single confocal plane is shown. Bars, 10 μ m. In panels A and B, right graphs represent measurements of Pearson's coefficient for mEGFP-mCherry colocalization at the 3D IS contact areas over the conjugation period. Measurements were performed on time-lapse stack confocal images from the CD3 ζ -mEGFP and CD81-mCherry (A) or ICAM-1-mEGFP and CD81-mCherry (B) IS, as in the examples depicted in the left panels. Data are means \pm standard errors of the means of 16 (A) and 11 (B) cells ($n = 2$ independent experiments each).

CD3 ζ -mEGFP) and CD81-mCherry as the acceptor. Cells were conjugated with Raji/SEE cells and imaged. The fluorescence lifetime of donor mEGFP-fused constructs in cotransfected cells was compared with that in control cells expressing only mEGFP-tagged donor molecules. Donor-acceptor interactions were measured as the localization and percentage of the number of pixels detected at the highest FRET efficiency (FRETeff) for each pair, which can vary as a function of the distance between the two fluorophores and/or the affinity between the proteins. Phasor-FLIM-FRET analysis of ICAM-3-mEGFP and CD81-mCherry pairs, used as the negative control, showed an average FRETeff value similar to that of the donor fluorophore alone, and the percentage of pixels with FRETeff above the uncertainty of the measurement was negligible (see Fig. S2A in the supplemental

material). PhasorFLIM-FRET analysis revealed a CD81-CD9 heterophilic interaction in nonconjugated cells (Fig. 4A; see also Fig. S2B in the supplemental material), in agreement with previous biochemical data (46, 47). Tetraspanin CD9 was also enriched at the IS, displaying different IS relocalization kinetics in comparison to those of CD81 (see Fig. S3 in the supplemental material). Interestingly, the CD81-CD9 interaction was enhanced by cell-cell conjugation (Fig. 4A), suggesting that conjugation prompted stronger TEM interactions. In nonspecific contacts, with no CD9 clustering in the contact area, the extent of the CD9-CD81 interaction was similar to that in nonconjugated cells. The extent of the association increased progressively during IS formation, from initial cognate contacts to the early cSMAC and throughout the contact in the late IS (Fig. 4A).

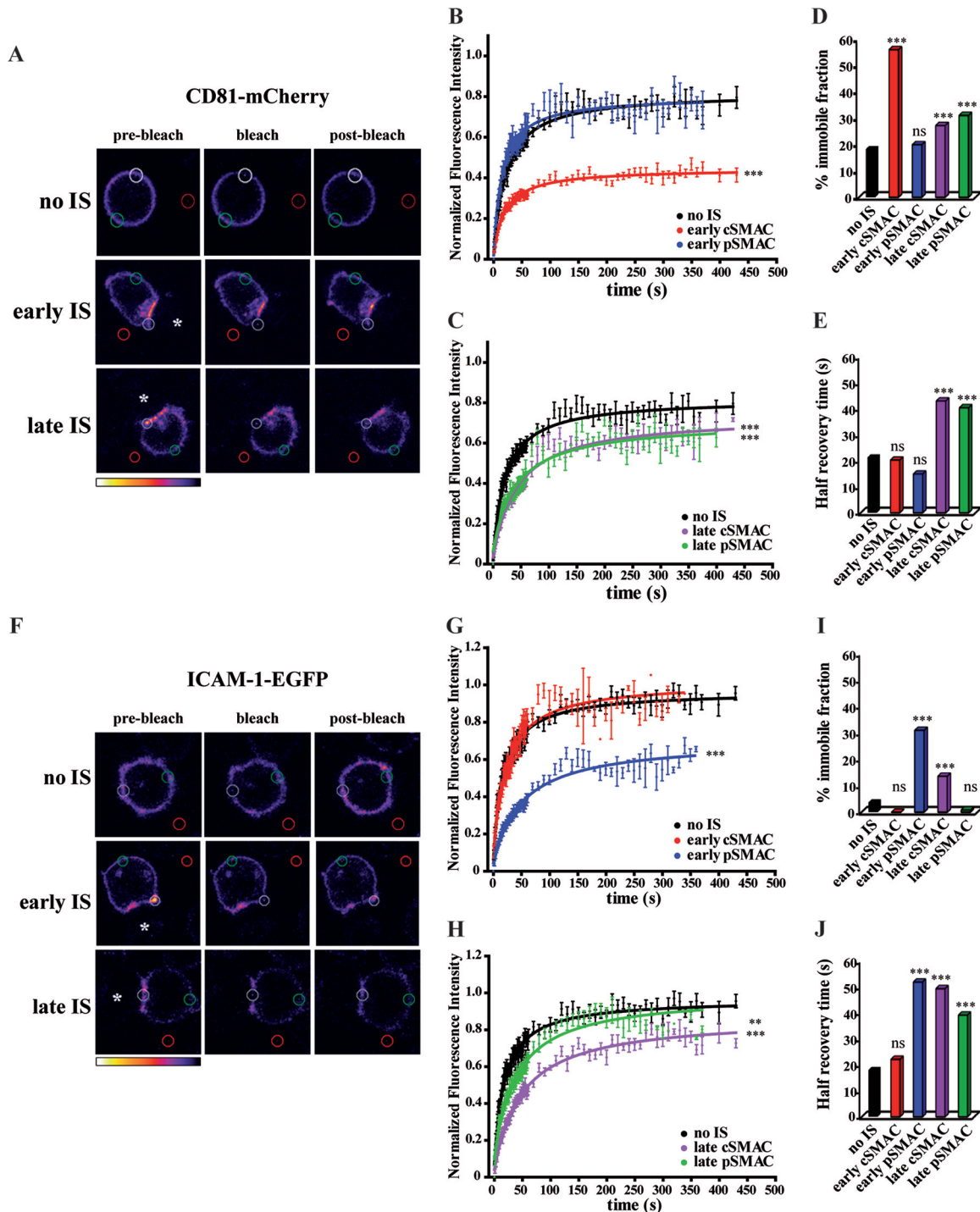


FIG 3 CD81 and ICAM-1 dynamics at the IS. J77/CD81-mCherry (A to E) or J77/ICAM-1-mEGFP (F to J) cells were conjugated with Raji/SEE cells (asterisks). FRAP was conducted on the cSMAC or pSMAC of early and late ISs and on nonconjugated T cells. Data were analyzed by one-way ANOVA with Tukey's *post hoc* multiple-comparison test. (A) Example prebleach, bleach, and final postbleach images depicted in pseudocolor intensity-coding format (maximum intensity in white): white circles, bleached areas; green circles, membrane areas distant from the bleached areas, used as an internal control; red circles, background. (B) Mean-fitted fluorescence recovery curves \pm standard errors of the means for nonconjugated cells ($n = 12$), the cSMAC ($n = 11$), and the pSMAC ($n = 10$) of the early IS. (C) Mean-fitted fluorescence recovery \pm standard error of the mean in nonconjugated cells (same curve as in panel B), the cSMAC ($n = 9$), and the pSMAC ($n = 13$) of the late IS. (D and E) Bar histograms showing the immobile fractions (D) and half-recovery times (E) calculated from the fitted curves. (F) Example pseudocolored images depicted as described above for panel A. (G) Mean-fitted fluorescence recovery curves \pm standard errors of the means for nonconjugated cells ($n = 15$), the cSMAC ($n = 11$), and the pSMAC ($n = 12$) of the early IS. (H) Mean-fitted fluorescence recovery in nonconjugated cells (curve as in panel G), the cSMAC ($n = 10$), and the pSMAC ($n = 10$) of the late IS. (I and J) Bar histograms showing the immobile fractions (I) and half-recovery times (J). ns, not significant.

TABLE 1 Derived apparent diffusion coefficients for CD81-mCherry and ICAM-1-mEGFP in nonconjugated T cells and in different areas and phases of the IS

Phase and area	Mean D ($\mu\text{m}^2/\text{s}$) \pm SD ^a	
	CD81-mCherry	ICAM-1-mEGFP
No IS	0.42 \pm 0.04	0.46 \pm 0.05
Early cSMAC	0.44 \pm 0.11	0.38 \pm 0.15
Early pSMAC	0.60 \pm 0.17	0.16 \pm 0.04
Late cSMAC	0.21 \pm 0.05	0.17 \pm 0.03
Late pSMAC	0.22 \pm 0.06	0.21 \pm 0.05

^a D , derived apparent diffusion coefficient.

CD81 colocalization with ICAM-1 increased with the progression of IS cell-cell conjugation (Fig. 2B). We then assessed the ICAM-1-CD81 molecular interaction by phasorFLIM-FRET. Analysis of the ICAM-1-CD81 donor-acceptor pair in nonconjugated cells revealed a low percentage of pixels at high FRETeff (see Fig. S2B in the supplemental material). A clear increase in this percentage was observed in initial cognate contacts (Fig. 4B), despite the lack of clear ICAM-1 redistribution to the contact area. As conjugation progressed, the percentage of high-FRETeff pixels increased, first at the early IS and then throughout the late IS

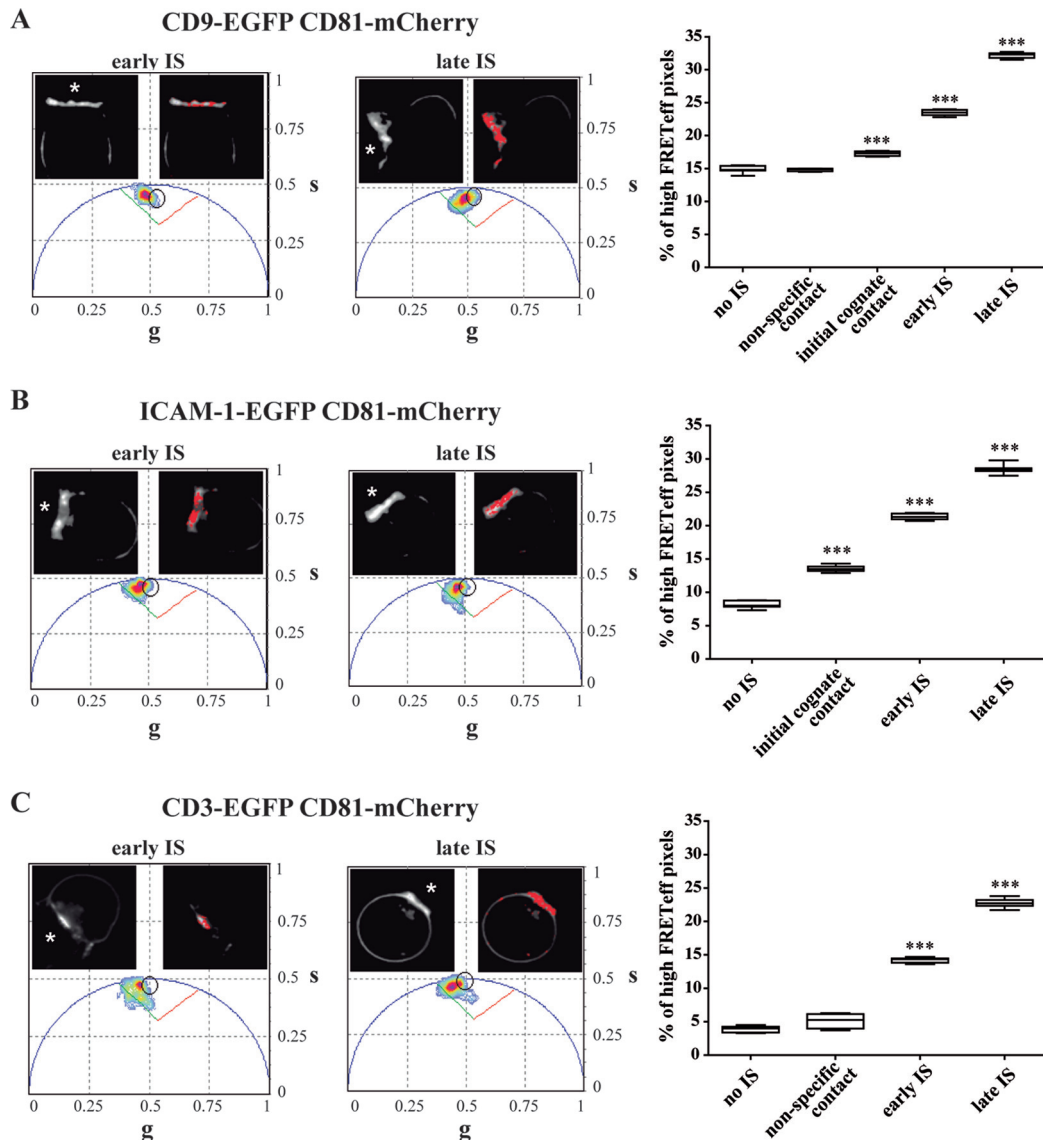


FIG 4 CD81 interaction with ICAM-1 and CD3 at the IS. J77 cells cotransfected with mEGFP-mCherry pairs were conjugated with Raji/SEE cells and analyzed by phasorFLIM-FRET. Data were analyzed by one-way ANOVA with Bonferroni's *post hoc* multiple-comparison test. (A) Examples of FRET-FLIM detection of the CD9-CD81 pair in early and late ISs (the asterisks mark the Raji B cell location). In each chart, the EGFP lifetime distribution is shown in the phasor plot, where the green and red lines mark 0 and 50% FRETeff, respectively. The black circular cursor in the phasor plot selects the subset of pixels shown in the correlated FLIM images by the red mask (right-hand image inside each chart). mEGFP fluorescence intensity is depicted in grayscale (left-hand image inside each chart). The graph shows quantification of the percentage of high-FRETeff pixels for no IS (T cells alone) ($n = 7$), nonspecific contact ($n = 4$), initial cognate contact ($n = 7$), the early IS ($n = 7$), and the late IS ($n = 7$). (B) Examples of FRET-FLIM detection for the ICAM-1-CD81 pair in early and late ISs, analyzed as described above for panel A. The graph shows quantification of the percentage of high-FRETeff pixels: no IS ($n = 8$), initial cognate contact ($n = 12$), the early IS ($n = 5$), and the late IS ($n = 12$). (C) Examples of FRET-FLIM detection for the CD3 ζ -CD81 pair in early and late ISs, analyzed as described above for panel A. The graph shows quantification of the percentage of high-FRETeff pixels: no IS ($n = 6$), nonspecific T cell-B cell contact ($n = 4$), the early IS ($n = 10$), and the late IS ($n = 20$).

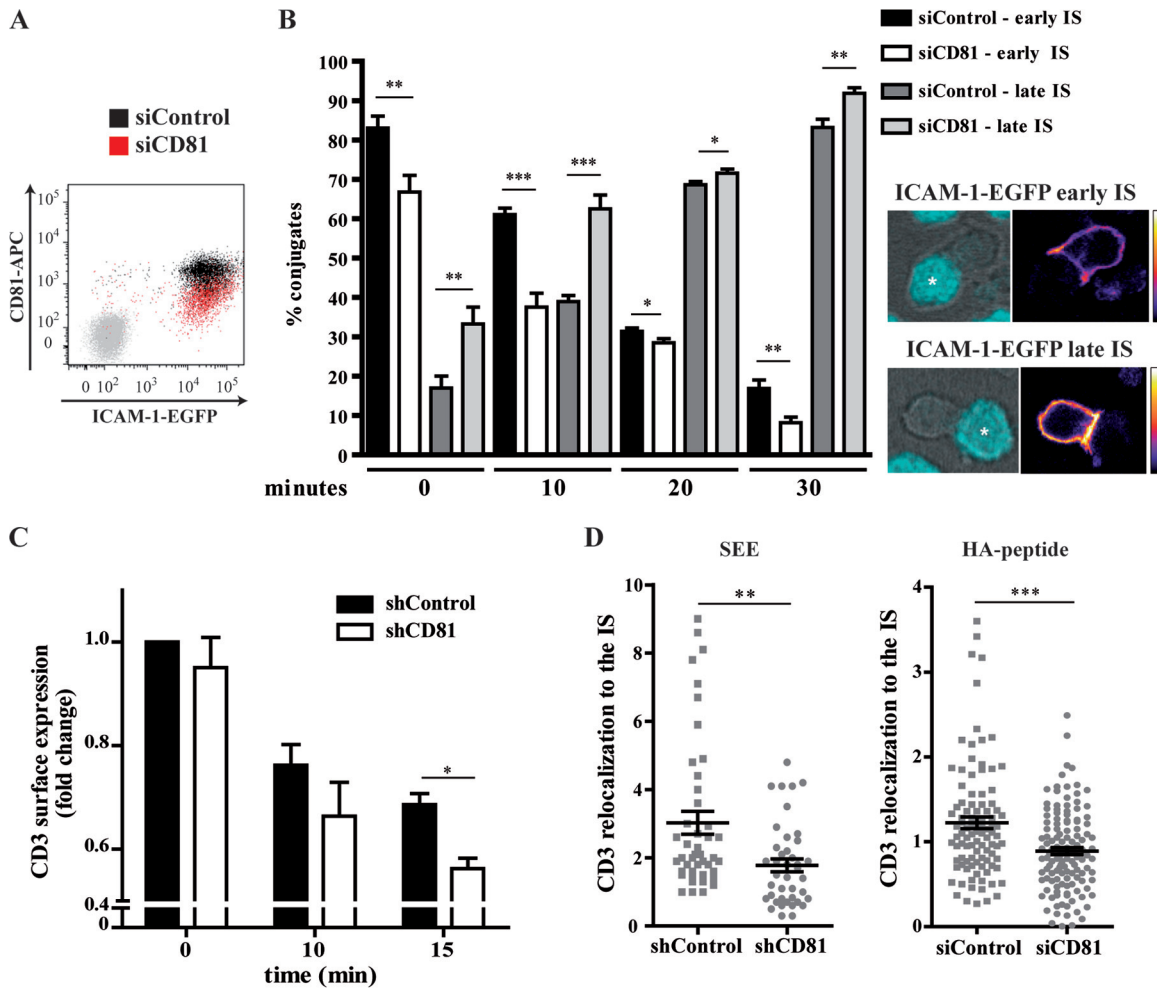


FIG 5 CD81 controls IS organization. (A) J77 cells were cotransfected with control siRNA or siCD81 and ICAM-1-mEGFP, stained for CD81, and analyzed by flow cytometry. The negative control, in gray, represents cells stained only with secondary antibody. (B) J77/ICAM-1-mEGFP cells treated with control or CD81 siRNA were conjugated with Raji/SEE cells, and the percentage of conjugates in the early or late IS (monitored by ICAM-1 distribution) was quantified. Data are means \pm standard errors of the means of 100 contacts ($n = 3$ independent experiments). Right panels are example pseudocolored images of the ICAM-1-mEGFP distribution and merged bright-field and blue channels (Raji/SEE) (asterisks). (C) J77/shControl or J77/shCD81 cells were incubated with Raji/SEE cells for the indicated times. Data represent the fold changes in CD3 surface expression levels with respect to levels in shControl cells in the presence of nonactivated Raji cells (0 min) and are shown as means \pm standard errors of the means ($n = 5$ in triplicate). (D) J77/shRNA T cells were conjugated with Hom2/HA B cells (HA peptide) (right) for 20 min, and CD3 relocation to the IS was measured. Data are means \pm standard errors of the means of 50 (SEE) and 100 (HA) conjugates ($n = 2$ independent experiments each).

contact, indicating ICAM-1 and CD81 molecular interactions during IS progression (Fig. 4B). This increase in the CD81-ICAM-1 association correlates directly with the increase in CD81-ICAM-1 colocalization during IS maturation (Fig. 2B).

Since CD81 colocalized with CD3 at the IS (Fig. 2A), we also analyzed the possible interaction between these proteins. In nonconjugated cells, the average FRETeff value was below the detection limit of the technique, suggesting negligible CD3-CD81 molecular interactions (see Fig. S2B in the supplemental material). However, we detected a very low percentage of pixels at high FRETeff, which remained unchanged in nonspecific contacts (Fig. 4C). In the early IS, the percentage of high-FRETeff CD3-CD81 pixels in the cSMAC was significantly increased, and the late IS displayed the greatest extent of interaction (Fig. 4C), suggesting that these molecules are in close proximity as they spread from the cSMAC throughout the contact. Although CD81 and CD3

showed a high level of colocalization at all times (Fig. 2A), phasor-FLIM-FRET analysis indicated that direct protein-protein interactions increase with the progression of the IS cell-cell contact (Fig. 4C).

Together, these results show that CD81-CD3, CD81-ICAM-1, and CD81-CD9 molecular interactions are induced progressively during IS maturation.

Role of CD81 in the organization of the mature IS. We studied the effect of CD81 silencing on the dynamics of IS constituents. J77/ICAM-1-mEGFP cells transfected with control or CD81 siRNA (siCD81) (Fig. 5A) were conjugated with Raji/SEE cells for different times and plated onto PLL-coated coverslips for 15 min (Fig. 5B). We used ICAM-1-mEGFP to categorize the IS as an early IS (pSMAC enrichment) (Fig. 5B, right) or late IS (enrichment throughout the contact) (bottom right). CD81 knockdown decreased the proportion of early ISs while increasing the propor-

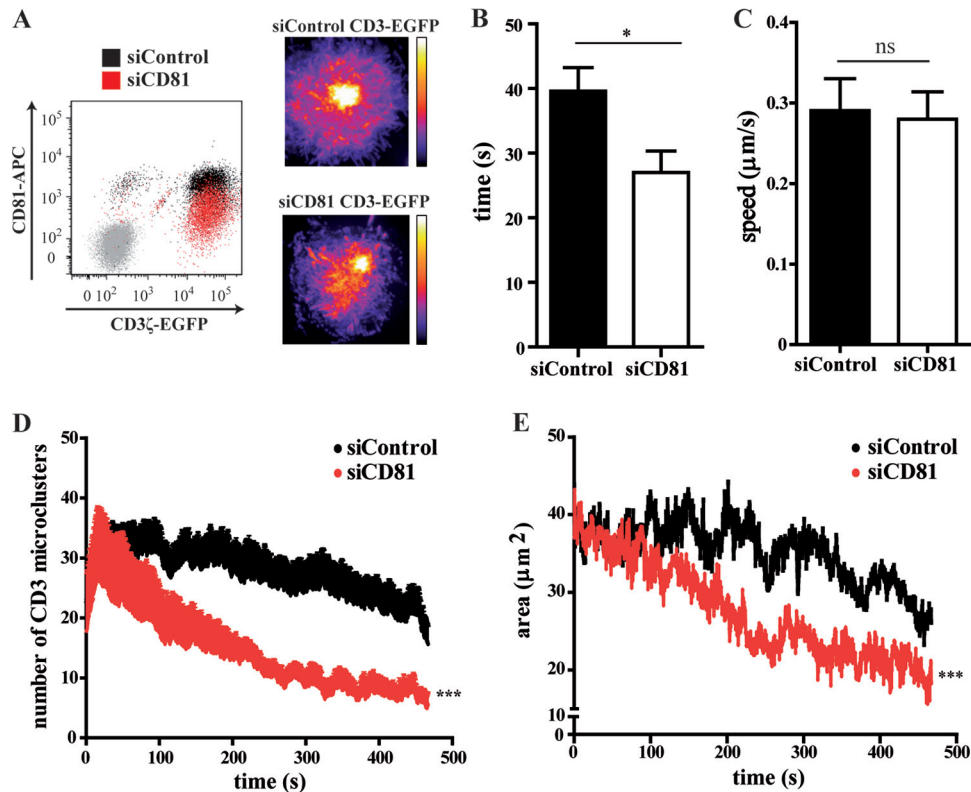


FIG 6 CD81 regulates CD3 dynamics at the IS. (A, left) Flow cytometry analysis of J77 cells cotransfected with control siRNA or siCD81 and CD3ζ-mEGFP and stained for CD81. The negative control, in gray, represents cells stained only with secondary antibody. J77/CD3ζ-mEGFP cells treated with siControl or siCD81 were plated onto CD3-coated coverslips and analyzed by TIRFM. (Right) Example pseudocolor images of time-maximal projections of CD3ζ-mEGFP microclusters at the cell membrane of siRNA-treated cells. (B to E) Graphs showing the duration of detection of each CD3 microcluster (B), the speed mean of the tracks (C), and, at each time point, the number of microclusters (D) and the cSMAC area (E). Data are means ± standard errors of the means for 8 cells under each condition ($n = 2$ independent experiments).

tion of late synapses (Fig. 5B), strongly indicating that CD81 regulates IS maturation and ICAM-1 reorganization at the contact.

Next, we assessed the role of CD81 in CD3 reorganization. After 15 min of conjugation with Raji/SEE cells, CD81-silenced cells displayed lower levels of endogenous surface CD3 than did control cells (Fig. 5C). Moreover, this decrease was accompanied by impaired CD3 relocalization to the IS with respect to the rest of the cell membrane in 20-min conjugates (Fig. 5D, left). This decrease in CD3 relocalization upon CD81 silencing was confirmed with antigen-specific conjugates formed between CD81-silenced CH7C17 T cells and Hom2 B cells loaded with HA peptide and labeled with CMAC cell tracker (Hom2/HA cells) (Fig. 5D, right). The role of CD81 in CD3 dynamics was further analyzed by total internal reflection fluorescence microscopy (TIRFM). J77/CD3ζ-mEGFP cells transfected with siControl or siCD81 (Fig. 6A, left) were plated onto anti-CD3-coated coverslips, and CD3 microcluster dynamics was investigated (Fig. 6A; see also Video S1 in the supplemental material). Although TCR microclusters are stationary due to the immobility of the stimulating ligand on the glass, there is protein flux in and out the assembled clusters (48) (see Video S1 in the supplemental material), and the cSMAC formed correctly in many cells (Fig. 6A, right). Interestingly, CD3 microclusters at CD81-silenced cell membranes disappeared from the TIRFM depth detection range (~90 nm) more rapidly (Fig. 6B), while their tracks displayed an equal average speed (Fig. 6C), in-

dicating cluster internalization rather than movement to other membrane regions outside the imaging field. Therefore, we also observed a time-dependent reduction in the number of microclusters (Fig. 6D) and cSMAC areas (Fig. 6E) in CD81-silenced cells. These experiments suggest that CD81-CD3 interactions are required for efficient retention of the CD3 signaling complex in T cell plasma membranes during cognate interactions.

CD81 controls the T cell activation threshold. IS organization in the absence of CD81 was further investigated by using two different CD81 shRNA sequences, obtaining similar phenotypes (Fig. 7A and data not shown). Surface expression levels of different molecules were not significantly altered by CD81 silencing in nonconjugated T cells (Fig. 7B). CD81 downregulation reduced the total number of SEE-dependent conjugates (Fig. 7C), without differences in contact duration (data not shown). CD81-depleted cells displayed impaired microtubule-organizing center (MTOC) translocation to the IS, with increased distance to the APC surface (Fig. 7D). Moreover, CD81 downregulation enhanced F-actin relocalization to the IS (Fig. 7E), despite similar F-actin polymerization rates in control and CD81-silenced cells (Fig. 7F).

In the context of T cell-APC cognate interactions, CD81 downmodulation not only altered IS organization but, as a consequence, also impaired signaling and T cell activation. Indeed, CD81 silencing reduced the levels of CD3ζ, ZAP-70, LAT, and extracellular signal-regulated kinase (ERK) phosphorylation with

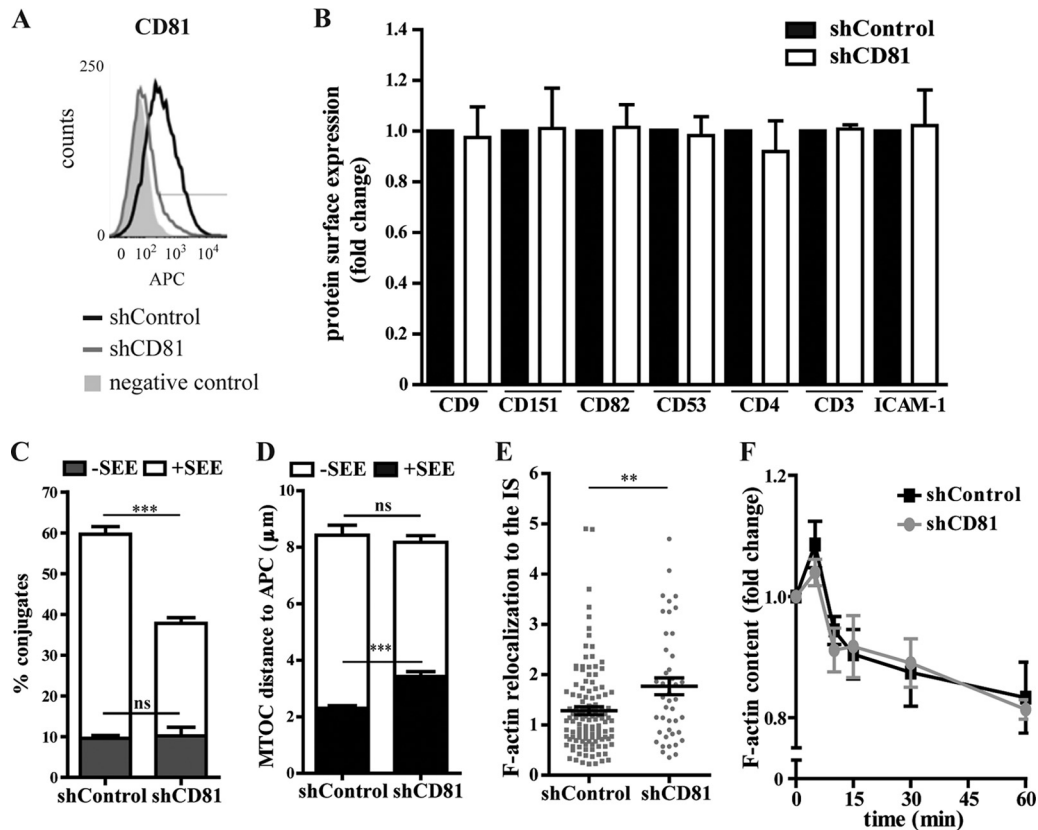


FIG 7 CD81 controls IS formation. (A) J77 cells were transduced with CD81 shRNA or an empty vector (shControl), stained for CD81, and analyzed by flow cytometry. The negative control represents cells stained only with secondary antibody. (B) Expression levels of membrane proteins determined by flow cytometry in T cells depleted for CD81 or not (shControl). Variations were not statistically significant. Data are presented as fold changes with respect to the expression levels of each protein in control cells and are shown as means \pm standard deviations from three independent experiments. (C) J77/shRNA cells were incubated with Raji/+SEE or Raji/-SEE cells for 20 min, and the percentage of T cell-B cell contacts was quantified. Data are means \pm standard errors of the means for 100 contacts ($n = 3$ independent experiments), determined by one-way ANOVA with Bonferroni's *post hoc* multiple-comparison test. (D) J77/shRNA cells were conjugated with Raji/+SEE or Raji/-SEE cells for 20 min and stained with antitubulin. Data are the MTOC distances from the IS (μm) and are shown as means \pm standard errors of the means for 100 conjugates ($n = 3$ independent experiments), determined by one-way ANOVA with Bonferroni's *post hoc* multiple-comparison test. (E) J77/shRNA cells were conjugated with Raji/SEE cells for 20 min, and F-actin relocation to the IS was measured. Data are means \pm standard errors of the means for 50 conjugates ($n = 2$ independent experiments). (F) J77/shRNA cells were stimulated with anti-CD3, fixed, labeled with phalloidin, and analyzed by flow cytometry. Data are the fold changes in F-actin content with respect to the expression level in the absence of the antibody (0 min) and are shown as means \pm standard errors of the means ($n = 3$ independent experiments performed in triplicate).

the time of conjugation (Fig. 8A). A reduction in the level of CD3 downstream intracellular signaling during IS maturation was observed with conjugates formed between CD81-silenced J77 T cells and Raji/SEE B cells as well as with antigen-specific conjugates formed between CD81-silenced CH7C17 T cells and Hom2/HA B cells (Fig. 8A). CD81-silenced T cells also showed lower membrane expression levels of the T cell activation marker CD69 (Fig. 8B) and reduced IL-2 secretion (Fig. 8C) in both J77/Raji and CH7/Hom2 conjugation systems.

In order to directly assess the role of CD81-mediated signaling in T cell activation, CH7C17 T cells were treated with fluorescently labeled cell-permeable peptides corresponding to the C-terminal sequence of CD81 or with a scrambled combination of the same 8 amino acids as a control. Treated T cells were then conjugated with Hom2/HA cells, and T cell activation was measured by quantifying CD69 expression levels (Fig. 8D). Treatment of T cells with peptides containing the C-terminal sequence of CD81 did not affect T cell activation, suggesting that CD81 direct downstream signaling is not involved in T cell activation. Tetraspanin associa-

tions with several membrane proteins occur through their LEL extracellular domain (49), and GST proteins fused to the LEL extracellular domain (GST-LEL) of different tetraspanin molecules have been used to perturb functions regulated by tetraspanin microdomains, since they decrease the diffusion of tetraspanin molecules at the plasma membrane (19). Pretreatment of CH7C17 T cells with GST-LEL-CD81 before conjugation with Hom2/HA B cells induced an increase in the CD69 expression level in comparison with control GST alone (Fig. 8E), further indicating that CD81 regulates T cell activation by interacting with other membrane proteins through its extracellular domain rather than by its direct intracellular signaling.

Taken together, these results suggest that CD81 is important for the organization of CD3 at the IS and for CD3-mediated intracellular signaling, regulating proper T cell signaling and activation.

DISCUSSION

In this study, we provide evidence that CD81 controls IS formation and progression through its dynamic interaction with CD3

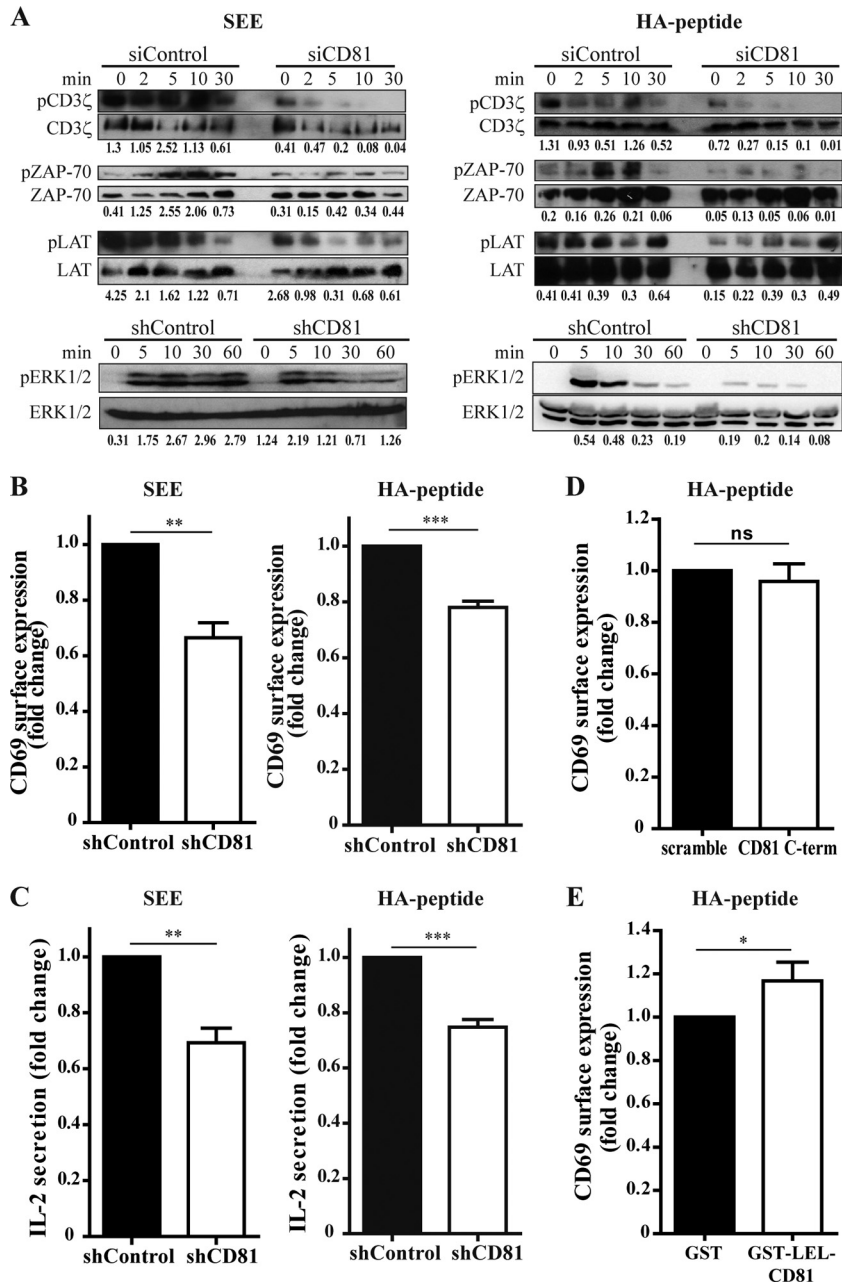


FIG 8 CD81 regulates the T cell activation threshold. (A) CD81-knocked-down J77 or CH7C17 T cells were conjugated for the indicated times with Raji/SEE (SEE) and Hom2/HA (HA-peptide) B cells, respectively. Cells were then lysed and immunoblotted for phosphorylated and total CD3 ζ , ZAP-70, LAT, and ERK1/2. Blots are from a representative experiment out of three; numbers below the blots indicate the phosphorylated/total signal ratio. (B and C) J77/shRNA and Raji/SEE or CH7/shRNA and Hom2/HA cells were conjugated for 16 h. (B) Cells were labeled for CD69 and analyzed by flow cytometry. Data are the fold changes in CD69 surface expression levels with respect to levels in shControl cells and are shown as means \pm standard errors of the means ($n = 4$ [SEE] and $n = 5$ [HA] independent experiments). (C) Supernatants were analyzed by an enzyme-linked immunosorbent assay. Data are the fold changes in levels of secreted IL-2 with respect to those in shControl cells and are shown as means \pm standard errors of the means ($n = 3$ [SEE] and $n = 4$ [HA] independent experiments). (D) CH7 T cells preincubated with permeable CD81 or scrambled peptides were conjugated with Hom2/HA cells for 16 h. Data are the fold changes in CD69 surface expression levels with respect to those in control cells and are shown as means \pm standard errors of the means ($n = 2$ independent experiments). (E) CH7 T cells preincubated with GST alone or GST-LEL-CD81 fusion proteins were conjugated with Hom2/HA cells for 16 h. Data are the fold changes in CD69 surface expression levels with respect to control cells and are shown as means \pm standard errors of the means ($n = 2$ independent experiments).

and ICAM-1. A recent electron microscopy study of mouse ISs, from contacts for up to 6 h, identified four distinct morphological stages. Initial synapses (10 to 30 min) were characterized by contacts through pseudopodia, while later phases corresponded to

specific distributions of intracellular structures at the IS area (50). Previous descriptions of IS dynamics indicated that protein polarization reaches a maximum by ~ 30 min (51), with increasing interaction forces (52). T cells sustain the IS ring pattern for over

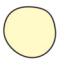


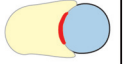
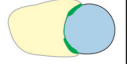


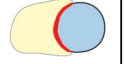

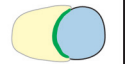
	Time (min)	CD81 distribution	ICAM-1 distribution	CD3 distribution
non-conjugated				
non-specific contact				
initial cognate contact	~ 0 - 2			
early IS	~ 2 - 10			
	~ 10 - 20			
late IS	~ 20 - 40			
	~ 50			

FIG 9 Definition of IS stages based on protein redistribution (CD81, ICAM-1, and CD3) at the T cell-APC contact area during 1 h of conjugation: initial cognate contacts, characterized by membrane contacts between polarized T cells and stimulated APCs; the early IS, showing differential protein enrichment at the cSMAC (CD3 and CD81) or the pSMAC (ICAM-1); and the late IS, with even protein distribution throughout the IS contact area.

1 h when plated onto lipid bilayers (53). In our analysis, we examined live T cell-B cell conjugates and discerned different IS steps not detected in previous studies. IS stages were defined based on protein redistribution, dynamics, and interactions at the contact area during 1 h of conjugation, delineating three major IS stages: initial cognate contacts, between polarized T cells and stimulated APCs; the early IS, showing differential protein enrichment at the cSMAC or pSMAC; and the late IS, with proteins evenly distributed throughout the IS and showing high protein-protein interaction levels (Fig. 9). Our data point to a regulation of the dynamics of synapse architectural organization not only by size differences in ectodomains of cell surface proteins (54) but also by protein-protein interactions driven by TEMs.

This novel stepwise IS formation reveals an important role for CD81. Our data indicate a correlation between colocalization and protein-protein molecular interaction studies, with an increase in the extent of CD81 associations as conjugation progressed, although the full extent of interactions is underestimated in our phasorFLIM-FRET experiments due to the competition with endogenous untagged proteins. In early synapses, most CD81 is engaged at the cSMAC, where it colocalizes and interacts directly with CD3. In accordance, CD81 association with the CD3 δ subunit was recently identified by a yeast two-hybrid screen (55). Remarkably, at the same stage, ICAM-1, which is initially enriched at the pSMAC, progressively redistributes throughout the contact, with an increase in colocalization and a concomitant increase in direct associations with CD81 molecules. The high level of immobility of CD81 and ICAM-1 molecules in this early stage indicates that protein redistribution during IS progression could be regulated by interactions with the cytoskeleton. In late synapses, CD81

redistributes evenly throughout the IS, showing similar dynamics in the cSMAC and pSMAC, and colocalization and protein-protein interactions with CD3 and ICAM-1 are detected over a larger area. In this IS stage, slow protein dynamics and high levels of membrane protein-protein interactions suggest that IS protein enrichment is regulated by interactions within TEMs. Cytoskeleton polarization toward cell-cell contacts is crucial for the formation of the mature IS (56, 57). Accordingly, treatment of J77 T cells with the actin-depolymerizing toxin latrunculin A before incubation with Raji/SEE cells prevented IS formation, with the very few T cell-B cell contacts observed being devoid of CD81-mCherry or endogenous CD3 accumulation at the IS (data not shown), in agreement with previous works (5, 58). Cholesterol is an essential component of TEMs (46), with an important role in the IS context (59–62). T cell-B cell conjugation as well as CD81 and CD3 accumulation at the IS were also significantly reduced by the treatment of J77 T cells with methyl- β -cyclo-dextrin, a drug that extracts membrane cholesterol, before incubation with Raji/SEE cells (data not shown). TEMs might then modulate IS organization and maturation by mediating the link between membrane proteins and lipids, cytoskeleton components, and signaling molecules.

CD81 diffusion properties in nonconjugated T cells are similar to those of ICAM-1, in agreement with previous studies showing comparable apparent diffusion coefficients for ICAM-1 and tetraspanins CD9 and CD151 in nude endothelial cell plasma membranes (19). We also observed similarities in ICAM-1 and CD81 diffusion properties in the late IS. The mobility of tetraspanins CD63 and CD82 is comparable to the one of MHCII in late endosomal multivesicular bodies (63), and it is possible that their diffusional behavior also varies according to IS sublocalization and maturation stages. Although CD81 is also present in intracellular vesicles and is secreted through exosomes (64), CD81 is expressed mainly on the plasma membrane of T cells. To study CD81 and ICAM-1 dynamics, we have chosen small bleaching areas ($\sim 8.5 \mu\text{m}^2$) located specifically at the T cell plasma membrane.

CD81 regulates the correct timing of IS maturation. CD81 downregulation accelerates the proportion of late IS conjugates (based on the ICAM-1 distribution pattern) and reduces CD3 relocalization to the IS, enhancing CD3 microcluster internalization following TCR stimulation. TCR microcluster movement (53) and signal termination (5) are controlled by the actin cytoskeleton. CD81 could mediate functional interactions between actin and CD3 or ICAM-1. On the IS APC side, continuous ICAM-1 recycling is controlled by LFA-1, actin, and microtubules (65). In B cells, CD81 microdomains alongside the actin cytoskeleton play a key role in regulating CD19 mobility and in organizing CD19 and B cell receptor (BCR) interactions that lead to BCR signaling (66). CD81 is connected to the actin cytoskeleton through its association with ezrin-radixin-moesin (ERM) proteins (67), which are recruited to the IS and play a role in T cell activation (68). F-actin dynamics is also regulated by Rho GTPases (69), and CD81 was recently shown to associate directly with the small GTPase Rac-1 (70, 71). However, our data for CD81 C-terminal cell-permeable peptides and soluble GST-LEL-CD81 fusion proteins suggest that the role of CD81 as an IS organizer might be related to its ability to interact with other transmembrane proteins, regulating their diffusional properties and subcellular localization rather than direct signaling or anchoring to the cytoskeleton through its C-terminal domain. Moreover, the opposite effects observed with CD81 silencing, which accelerates IS matu-

ration, and GST-LEL-CD81, which slows down diffusion of TEM proteins, indicate that CD81 microdomains regulate the time of permanence of TCR signaling at the IS plasma membrane, modulating the TCR signaling threshold.

Thus, as an IS organizer, CD81 regulates T cell activation. CD81-silenced T cells display reduced MTOC translocation toward the IS, which is TCR dependent (72) and necessary for full T cell activation (73) but independent of actin polarization (74). CD81 silencing reduces TCR downstream signaling, decreasing CD3 ζ , ZAP-70, LAT, and ERK1/2 phosphorylation, in agreement with data showing that CD81 T cell costimulation activates TCR ζ and ERK more strongly than does CD28 (75). Also, CD81-knocked-down T cells have reduced IL-2 secretion, which is dependent on ERK1/2 activation (76), and express lower levels of the T cell activation marker CD69. This observed decrease in T cell activation in CD81-silenced human T cells may seem contradictory with previous data showing hyperproliferative responses of CD81^{-/-} mouse T cells to CD3 cross-linking (55, 77). However, it is important to note that there are fundamental differences in the CD81 expression patterns between the two species. Opposite to human T cells, CD81 is expressed in mouse T cells only after T cell activation (37, 78). Recently, noncanonical T cell stimulation with antibodies against CD4 and the TCR showed a slight increase in CD69 expression levels in CD81-silenced T cells (55). This difference from our results is probably related to different T cell activation protocols. In our work, we have stimulated CD81-silenced T cells through antigen presentation by APCs by using two different conjugation systems (Raji/SEE and Hom2/HA cells), obtaining similar results with both. Moreover, in agreement with our results, CD81^{-/-} T cells do not develop Th2 responses when activated by antigen-presenting B cells, with reduced IL-4 production (79), and CD81 acts as a T cell-costimulatory molecule in human T cells (37, 38, 75).

TEMs accommodate numerous molecules, allowing the regulation of receptor avidity. Our findings provide evidence that CD81 regulates IS molecular organization by associating with CD3 and ICAM-1, controlling their segregation in the cSMAC and pSMAC over the course of IS maturation. The role of CD81 as a microdomain organizer is thus important for synapse maturation timing and necessary for a correct T cell signaling threshold that leads to full T cell activation.

ACKNOWLEDGMENTS

This work was supported by SAF2011-25834 from the Spanish Ministry of Science and Innovation, INDISNET-S2011/BMD-2332 from the Comunidad de Madrid, Cardiovascular Network RD12-0042-0056 from the Instituto Salud Carlos III, and ERC-2011-AdG 294340-GENTRIS.

We declare that we have no competing financial interests.

We thank S. Bartlett for English editing, M. Vicente-Manzanares for critical reading, and Soraya López-Martín for technical support. Microscopy was performed at the CNIC Microscopy and Dynamic Imaging Unit.

REFERENCES

- Yokosuka T, Saito T. 2010. The immunological synapse, TCR microclusters, and T cell activation. *Curr. Top. Microbiol. Immunol.* 340:81–107.
- Dustin ML, Olszowy MW, Holdorf AD, Li J, Bromley S, Desai N, Widder P, Rosenberger F, van der Merwe PA, Allen PM, Shaw AS. 1998. A novel adaptor protein orchestrates receptor patterning and cytoskeletal polarity in T-cell contacts. *Cell* 94:667–677.
- Monks CR, Freiberg BA, Kupfer H, Sciaki N, Kupfer A. 1998. Three-dimensional segregation of supramolecular activation clusters in T cells. *Nature* 395:82–86.
- Lillemeier BF, Mortelmaier MA, Forstner MB, Huppa JB, Groves JT, Davis MM. 2010. TCR and Lat are expressed on separate protein islands on T cell membranes and concatenate during activation. *Nat. Immunol.* 11:90–96.
- Varma R, Campi G, Yokosuka T, Saito T, Dustin ML. 2006. T cell receptor-proximal signals are sustained in peripheral microclusters and terminated in the central supramolecular activation cluster. *Immunity* 25:117–127.
- Vardhana S, Choudhuri K, Varma R, Dustin ML. 2010. Essential role of ubiquitin and TSG101 protein in formation and function of the central supramolecular activation cluster. *Immunity* 32:531–540.
- Yokosuka T, Kobayashi W, Sakata-Sogawa K, Takamatsu M, Hashimoto-Tane A, Dustin ML, Tokunaga M, Saito T. 2008. Spatio-temporal regulation of T cell costimulation by TCR-CD28 microclusters and protein kinase C theta translocation. *Immunity* 29:589–601.
- Hsu CJ, Hsieh WT, Waldman A, Clarke F, Huseby ES, Burkhardt JK, Baumgart T. 2012. Ligand mobility modulates immunological synapse formation and T cell activation. *PLoS One* 7:e32398. doi:10.1371/journal.pone.0032398.
- Fooksman DR, Vardhana S, Vasiliver-Shamis G, Liese J, Blair DA, Waite J, Sacristan C, Victoria GD, Zanin-Zhorov A, Dustin ML. 2010. Functional anatomy of T cell activation and synapse formation. *Annu. Rev. Immunol.* 28:79–105.
- Mittelbrunn M, Yanez-Mo M, Sancho D, Ursa A, Sanchez-Madrid F. 2002. Cutting edge: dynamic redistribution of tetraspanin CD81 at the central zone of the immune synapse in both T lymphocytes and APC. *J. Immunol.* 169:6691–6695.
- Delaguillaumie A, Lagaudriere-Gesbert C, Popoff MR, Conjeaud H. 2002. Rho GTPases link cytoskeletal rearrangements and activation processes induced via the tetraspanin CD82 in T lymphocytes. *J. Cell Sci.* 115:433–443.
- Engering A, Pieters J. 2001. Association of distinct tetraspanins with MHC class II molecules at different subcellular locations in human immature dendritic cells. *Int. Immunol.* 13:127–134.
- Imai T, Kakizaki M, Nishimura M, Yoshie O. 1995. Molecular analyses of the association of CD4 with two members of the transmembrane 4 superfamily, CD81 and CD82. *J. Immunol.* 155:1229–1239.
- Kropshofer H, Spindeldreher S, Rohn TA, Platania N, Grygar C, Daniel N, Wolpl A, Langen H, Horejsi V, Vogt AB. 2002. Tetraspanin microdomains distinct from lipid rafts enrich select peptide-MHC class II complexes. *Nat. Immunol.* 3:61–68.
- Shibagaki N, Hanada K, Yamashita H, Shimada S, Hamada H. 1999. Overexpression of CD82 on human T cells enhances LFA-1/ICAM-1-mediated cell-cell adhesion: functional association between CD82 and LFA-1 in T cell activation. *Eur. J. Immunol.* 29:4081–4091.
- Hemler ME. 2005. Tetraspanin functions and associated microdomains. *Nat. Rev. Mol. Cell Biol.* 6:801–811.
- Yanez-Mo M, Barreiro O, Gordon-Alonso M, Sala-Valdes M, Sanchez-Madrid F. 2009. Tetraspanin-enriched microdomains: a functional unit in cell plasma membranes. *Trends Cell Biol.* 19:434–446.
- Boucheix C, Rubinstein E. 2001. Tetraspanins. *Cell. Mol. Life Sci.* 58:1189–1205.
- Barreiro O, Zamai M, Yanez-Mo M, Tejera E, Lopez-Romero P, Monk PN, Gratton E, Caiolfa VR, Sanchez-Madrid F. 2008. Endothelial adhesion receptors are recruited to adherent leukocytes by inclusion in preformed tetraspanin nanoplateforms. *J. Cell Biol.* 183:527–542.
- Espenel C, Margeat E, Dosset P, Arduise C, Le Grimellec C, Royer CA, Boucheix C, Rubinstein E, Milhiet PE. 2008. Single-molecule analysis of CD9 dynamics and partitioning reveals multiple modes of interaction in the tetraspanin web. *J. Cell Biol.* 182:765–776.
- Levy S, Shoham T. 2005. The tetraspanin web modulates immune-signalling complexes. *Nat. Rev. Immunol.* 5:136–148.
- Sanyal M, Fernandez R, Levy S. 2009. Enhanced B cell activation in the absence of CD81. *Int. Immunol.* 21:1225–1237.
- Imai T, Yoshie O. 1993. C33 antigen and M38 antigen recognized by monoclonal antibodies inhibitory to syncytium formation by human T cell leukemia virus type 1 are both members of the transmembrane 4 superfamily and associate with each other and with CD4 or CD8 in T cells. *J. Immunol.* 151:6470–6481.
- Mannion BA, Berditchevski F, Kraeft SK, Chen LB, Hemler ME. 1996. Transmembrane-4 superfamily proteins CD81 (TAPA-1), CD82, CD63, and CD53 specifically associated with integrin alpha 4 beta 1 (CD49/CD29). *J. Immunol.* 157:2039–2047.

25. Barreiro O, Yanez-Mo M, Sala-Valdes M, Gutierrez-Lopez MD, Ovalle S, Higginbottom A, Monk PN, Cabanas C, Sanchez-Madrid F. 2005. Endothelial tetraspanin microdomains regulate leukocyte firm adhesion during extravasation. *Blood* 105:2852–2861.
26. Bullard DC, Hu X, Schoeb TR, Collins RG, Beaudet AL, Barnum SR. 2007. Intercellular adhesion molecule-1 expression is required on multiple cell types for the development of experimental autoimmune encephalomyelitis. *J. Immunol.* 178:851–857.
27. Kim HR, Na BR, Kwon MS, Ko YS, Han WC, Jun CD. 2013. Dynamic motile T cells highly respond to the T cell stimulation via PI3K-Akt and NF-kappaB pathways. *PLoS One* 8:e59793. doi:10.1371/journal.pone.0059793.
28. Roy J, Audette M, Tremblay MJ. 2001. Intercellular adhesion molecule-1 (ICAM-1) gene expression in human T cells is regulated by phosphotyrosyl phosphatase activity. Involvement of NF-kappaB, Ets, and palindromic interferon-gamma-responsive element-binding sites. *J. Biol. Chem.* 276:14553–14561.
29. Kurzinger K, Reynolds T, Germain RN, Davignon D, Martz E, Springer TA. 1981. A novel lymphocyte function-associated antigen (LFA-1): cellular distribution, quantitative expression, and structure. *J. Immunol.* 127:596–602.
30. Segura E, Guerin C, Hogg N, Amigorena S, Thery C. 2007. CD8+ dendritic cells use LFA-1 to capture MHC-peptide complexes from exosomes in vivo. *J. Immunol.* 179:1489–1496.
31. Balkow S, Heinz S, Schmidbauer P, Kolanus W, Holzmann B, Grabbe S, Laschinger M. 2010. LFA-1 activity state on dendritic cells regulates contact duration with T cells and promotes T-cell priming. *Blood* 116:1885–1894.
32. Campanero MR, del Pozo MA, Arroyo AG, Sanchez-Mateos P, Hernandez-Caselles T, Craig A, Pulido R, Sanchez-Madrid F. 1993. ICAM-3 interacts with LFA-1 and regulates the LFA-1/ICAM-1 cell adhesion pathway. *J. Cell Biol.* 123:1007–1016.
33. de la Fuente H, Mittelbrunn M, Sanchez-Martin L, Vicente-Manzanares M, Lamana A, Pardi R, Cabanas C, Sanchez-Madrid F. 2005. Synaptic clusters of MHC class II molecules induced on DCs by adhesion molecule-mediated initial T-cell scanning. *Mol. Biol. Cell* 16:3314–3322.
34. James JR, Vale RD. 2012. Biophysical mechanism of T-cell receptor triggering in a reconstituted system. *Nature* 487:64–69.
35. Rodriguez-Plata MT, Puigdomenech I, Izquierdo-Useros N, Puertas MC, Carrillo J, Erkizia I, Clotet B, Blanco J, Martinez-Picado J. 2013. The infectious synapse formed between mature dendritic cells and CD4+ T cells is independent of the presence of the HIV-1 envelope glycoprotein. *Retrovirology* 10:42. doi:10.1186/1742-4690-10-42.
36. Tohma S, Hirohata S, Lipsky PE. 1991. The role of CD11a/CD18-CD54 interactions in human T cell-dependent B cell activation. *J. Immunol.* 146:492–499.
37. Todd SC, Lipps SG, Crisa L, Salomon DR, Tsoukas CD. 1996. CD81 expressed on human thymocytes mediates integrin activation and interleukin 2-dependent proliferation. *J. Exp. Med.* 184:2055–2060.
38. VanCompernelle SE, Levy S, Todd SC. 2001. Anti-CD81 activates LFA-1 on T cells and promotes T cell-B cell collaboration. *Eur. J. Immunol.* 31:823–831.
39. Martinez-Martin N, Fernandez-Arenas E, Cemurski S, Delgado P, Turner M, Heuser J, Irvine DJ, Huang B, Bustelo XR, Shaw A, Alarcon B. 2011. T cell receptor internalization from the immunological synapse is mediated by TC21 and RhoG GTPase-dependent phagocytosis. *Immunity* 35:208–222.
40. Montoya MC, Sancho D, Bonello G, Collette Y, Langlet C, He HT, Aparicio P, Alcover A, Olive D, Sanchez-Madrid F. 2002. Role of ICAM-3 in the initial interaction of T lymphocytes and APCs. *Nat. Immunol.* 3:159–168.
41. Gordon-Alonso M, Sala-Valdes M, Rocha-Perugini V, Perez-Hernandez D, Lopez-Martin S, Ursa A, Alvarez S, Kolesnikova TV, Vazquez J, Sanchez-Madrid F, Yanez-Mo M. 2012. EWI-2 association with alpha-actinin regulates T cell immune synapses and HIV viral infection. *J. Immunol.* 189:689–700.
42. Calabia-Linares C, Robles-Valero J, de la Fuente H, Perez-Martinez M, Martin-Cofreces N, Alfonso-Perez M, Gutierrez-Vazquez C, Mittelbrunn M, Ibiza S, Urbano-Olmos FR, Aguado-Ballano C, Sanchez-Sorzano CO, Sanchez-Madrid F, Veiga E. 2011. Endosomal clathrin drives actin accumulation at the immunological synapse. *J. Cell Sci.* 124: 820–830.
43. Caiola VR, Zamai M, Malengo G, Andolfo A, Madsen CD, Sutin J, Digman MA, Gratton E, Blasi F, Sidenius N. 2007. Monomer dimer dynamics and distribution of GPI-anchored uPAR are determined by cell surface protein assemblies. *J. Cell Biol.* 179:1067–1082.
44. Digman MA, Caiola VR, Zamai M, Gratton E. 2008. The phasor approach to fluorescence lifetime imaging analysis. *Biophys. J.* 94:L14–L16. doi:10.1529/biophysj.107.120154.
45. Zacharias DA, Violin JD, Newton AC, Tsien RY. 2002. Partitioning of lipid-modified monomeric GFPs into membrane microdomains of live cells. *Science* 296:913–916.
46. Charrin S, Manie S, Thiele C, Billard M, Gerlier D, Boucheix C, Rubinstein E. 2003. A physical and functional link between cholesterol and tetraspanins. *Eur. J. Immunol.* 33:2479–2489.
47. Kovalenko OV, Yang X, Kolesnikova TV, Hemler ME. 2004. Evidence for specific tetraspanin homodimers: inhibition of palmitoylation makes cysteine residues available for cross-linking. *Biochem. J.* 377:407–417.
48. Douglass AD, Vale RD. 2005. Single-molecule microscopy reveals plasma membrane microdomains created by protein-protein networks that exclude or trap signaling molecules in T cells. *Cell* 121:937–950.
49. Stipp CS, Kolesnikova TV, Hemler ME. 2003. Functional domains in tetraspanin proteins. *Trends Biochem. Sci.* 28:106–112.
50. Ueda H, Mophew MK, McIntosh JR, Davis MM. 2011. CD4+ T-cell synapses involve multiple distinct stages. *Proc. Natl. Acad. Sci. U. S. A.* 108:17099–17104.
51. Grakoui A, Bromley SK, Sumen C, Davis MM, Shaw AS, Allen PM, Dustin ML. 1999. The immunological synapse: a molecular machine controlling T cell activation. *Science* 285:221–227.
52. Hosseini BH, Louban I, Djandji D, Wabnitz GH, Deeg J, Bulbuc N, Samstag Y, Gunzer M, Spatz JP, Hammerling GJ. 2009. Immune synapse formation determines interaction forces between T cells and antigen-presenting cells measured by atomic force microscopy. *Proc. Natl. Acad. Sci. U. S. A.* 106:17852–17857.
53. Kaizuka Y, Douglass AD, Varma R, Dustin ML, Vale RD. 2007. Mechanisms for segregating T cell receptor and adhesion molecules during immunological synapse formation in Jurkat T cells. *Proc. Natl. Acad. Sci. U. S. A.* 104:20296–20301.
54. Burroughs NJ, Kohler K, Miloserdov V, Dustin ML, van der Merwe PA, Davis DM. 2011. Boltzmann energy-based image analysis demonstrates that extracellular domain size differences explain protein segregation at immune synapses. *PLoS Comput. Biol.* 7:e1002076. doi:10.1371/journal.pcbi.1002076.
55. Cevik SI, Keskin N, Belkaya S, Ozlu MI, Deniz E, Tazebay UH, Erman B. 2012. CD81 interacts with the T cell receptor to suppress signaling. *PLoS One* 7:e50396. doi:10.1371/journal.pone.0050396.
56. Beemiller P, Krummel MF. 2010. Mediation of T-cell activation by actin meshworks. *Cold Spring Harb. Perspect. Biol.* 2:a002444. doi:10.1101/cshperspect.a002444.
57. Billadeau DD, Nolz JC, Gomez TS. 2007. Regulation of T-cell activation by the cytoskeleton. *Nat. Rev. Immunol.* 7:131–143.
58. Campi G, Varma R, Dustin ML. 2005. Actin and agonist MHC-peptide complex-dependent T cell receptor microclusters as scaffolds for signaling. *J. Exp. Med.* 202:1031–1036.
59. Chichili GR, Westmuckett AD, Rodgers W. 2010. T cell signal regulation by the actin cytoskeleton. *J. Biol. Chem.* 285:14737–14746.
60. Gagnon E, Schubert DA, Gordo S, Chu HH, Wucherpfennig KW. 2012. Local changes in lipid environment of TCR microclusters regulate membrane binding by the CD3epsilon cytoplasmic domain. *J. Exp. Med.* 209: 2423–2439.
61. Gombos I, Kiss E, Detre C, Laszlo G, Matko J. 2006. Cholesterol and sphingolipids as lipid organizers of the immune cells' plasma membrane: their impact on the functions of MHC molecules, effector T-lymphocytes and T-cell death. *Immunol. Lett.* 104:59–69.
62. Van Komen JS, Mishra S, Byrum J, Chichili GR, Yaciuk JC, Farris AD, Rodgers W. 2007. Early and dynamic polarization of T cell membrane rafts and constituents prior to TCR stop signals. *J. Immunol.* 179:6845–6855.
63. Hoorn T, Paul P, Janssen L, Janssen H, Neefjes J. 2012. Dynamics within tetraspanin pairs affect MHC class II expression. *J. Cell Sci.* 125:328–339.
64. Mittelbrunn M, Gutierrez-Vazquez C, Villarroya-Beltri C, Gonzalez S, Sanchez-Cabo F, Gonzalez MA, Bernad A, Sanchez-Madrid F. 2011. Unidirectional transfer of microRNA-loaded exosomes from T cells to antigen-presenting cells. *Nat. Commun.* 2:282. doi:10.1038/ncomms1285.
65. Jo JH, Kwon MS, Choi HO, Oh HM, Kim HJ, Jun CD. 2010. Recycling

- and LFA-1-dependent trafficking of ICAM-1 to the immunological synapse. *J. Cell. Biochem.* 111:1125–1137.
66. Mattila PK, Feest C, Depoil D, Treanor B, Montaner B, Otipoby KL, Carter R, Justement LB, Bruckbauer A, Batista FD. 2013. The actin and tetraspanin networks organize receptor nanoclusters to regulate B cell receptor-mediated signaling. *Immunity* 38:461–474.
 67. Sala-Valdes M, Ursa A, Charrin S, Rubinstein E, Hemler ME, Sanchez-Madrid F, Yanez-Mo M. 2006. EWI-2 and EWI-F link the tetraspanin web to the actin cytoskeleton through their direct association with ezrin-radixin-moesin proteins. *J. Biol. Chem.* 281:19665–19675.
 68. Charrin S, Alcover A. 2006. Role of ERM (ezrin-radixin-moesin) proteins in T lymphocyte polarization, immune synapse formation and in T cell receptor-mediated signaling. *Front. Biosci.* 11:1987–1997.
 69. Vicente-Manzanares M, Sanchez-Madrid F. 2004. Role of the cytoskeleton during leukocyte responses. *Nat. Rev. Immunol.* 4:110–122.
 70. Quast T, Eppler F, Semmling V, Schild C, Homsy Y, Levy S, Lang T, Kurts C, Kolanus W. 2011. CD81 is essential for the formation of membrane protrusions and regulates Rac1-activation in adhesion-dependent immune cell migration. *Blood* 118:1818–1827.
 71. Tejera E, Rocha-Perugini V, Lopez-Martin S, Perez-Hernandez D, Bachir AI, Horwitz AR, Vazquez J, Sanchez-Madrid F, Yanez-Mo M. 2013. CD81 regulates cell migration through its association with Rac GTPase. *Mol. Biol. Cell* 24:261–273.
 72. Lowin-Kropf B, Shapiro VS, Weiss A. 1998. Cytoskeletal polarization of T cells is regulated by an immunoreceptor tyrosine-based activation motif-dependent mechanism. *J. Cell Biol.* 140:861–871.
 73. Martin-Cofreces NB, Robles-Valero J, Cabrero JR, Mittelbrunn M, Gordon-Alonso M, Sung CH, Alarcon B, Vazquez J, Sanchez-Madrid F. 2008. MTOC translocation modulates IS formation and controls sustained T cell signaling. *J. Cell Biol.* 182:951–962.
 74. Sedwick CE, Morgan MM, Jusino L, Cannon JL, Miller J, Burkhardt JK. 1999. TCR, LFA-1, and CD28 play unique and complementary roles in signaling T cell cytoskeletal reorganization. *J. Immunol.* 162:1367–1375.
 75. Sagi Y, Landrigan A, Levy R, Levy S. 2012. Complementary costimulation of human T-cell subpopulations by cluster of differentiation 28 (CD28) and CD81. *Proc. Natl. Acad. Sci. U. S. A.* 109:1613–1618.
 76. Genot E, Cleverley S, Henning S, Cantrell D. 1996. Multiple p21ras effector pathways regulate nuclear factor of activated T cells. *EMBO J.* 15:3923–3933.
 77. Miyazaki T, Muller U, Campbell KS. 1997. Normal development but differentially altered proliferative responses of lymphocytes in mice lacking CD81. *EMBO J.* 16:4217–4225.
 78. Maecker HT, Todd SC, Kim EC, Levy S. 2000. Differential expression of murine CD81 highlighted by new anti-mouse CD81 monoclonal antibodies. *Hybridoma* 19:15–22.
 79. Deng J, Dekruyff RH, Freeman GJ, Umetsu DT, Levy S. 2002. Critical role of CD81 in cognate T-B cell interactions leading to Th2 responses. *Int. Immunol.* 14:513–523.